Journal of Applied Polymer Science

Operating Window of Solution Casting, Part I: Newtonian Fluids

Yuan-Chan Huang, Tai-Zan Wang, Chi-Ping Tsai, Ta-Jo Liu
Department of Chemical Engineering, National Tsing Hua University, Hsinchu 30043, Taiwan, Republic of China
Correspondence to: T.-J. Liu (E-mail: tjliu@che.nthu.edu.tw)

ABSTRACT: An experimental study was carried out to investigate the fluid mechanics of solution casting. Newtonian glycerol solutions were used as test fluids and were casted on the polyethylene terephthalate films. The focus of this study is on the evaluation of the operating window, i.e., a region for stable and uniform processing. Different types of defects such as stable or unstable poolings, vibrating edges, and air entrainment outside the operating windows were observed. The effects of two different start-up approaches on the operating window were studied. One of the key operating parameters is the maximum casting velocity V_{max} for stable operation. The fluid viscosity is the most critical parameter on V_{max}. It was found that if the gap between the slot die exit and the moving film substrate is smaller than 600 μm, V_{max} might go down and then go up as the fluid viscosity increases. On the other hand, if the gap is larger than 600 μm, V_{max} will decrease as the fluid viscosity increases. Competition of two different types of defects, i.e., unstable pooling and air entrainment, can decide $V_{max,}$ as evidenced by the observation on the fluid motion and dynamic contact angles of different cases. The importance of different forces on V_{max} was also analyzed. © 2012 Wiley Periodicals, Inc. J. Appl. Polym. Sci. 129: 507–516, 2013

KEYWORDS: coatings; viscosity; viscoelasticity; films

Received 25 July 2012; accepted 19 September 2012; published online 22 November 2012
DOI: 10.1002/app.38617

INTRODUCTION

Polymer films that are widely used in various industrial applications are made by three processing methods; the first one is melt extrusion, such as the polyethylene terephthalate (PET) films.[1] The second method is film blowing molding,[2–6] such as plastic bags. The third method is usually called solution or solvent casting.[7] Many important polymer films that are needed for optical applications are made by solution casting processes. For example, polyimide (PI) films[8–11] and triacetyl cellulose (TAC) films[12–16] are made by the solution casting processes. The advantages of solvent casting include the high flatness of film uniformity can be achieved; polymer molecules can have isotropic arrangements; it is suitable for temperature-sensitive polymers; and excellent optical properties and low hazes of the polymer films can be retained. There have been extensive studies on the extrusion and blow molding processes.[1–6] However, the fundamental analysis on the solution casting process appears rare. The earliest patent on solvent casting was issued to Steven and Lefferts[17] on the production of celluloid film. Kinsella[18] used nickel-plated band to make cellulose diacetate film through continuous solvent casting operations. Juergen and Siemann[19] replaced the melt extrusion process by the solvent casting process so that the isotropic properties of polyarylate film products can be significantly improved. Recently, several authors examined the optical properties of the cast TAC,[20–24] PI,[11,25] and other polymer films.[26–28] Nakayama et al.[20] controlled TAC film's in-plane birefringence and out-of-plane birefringence. Hamamoto et al.[29] suggested to make high tensile and elongation of PI films by continuous solvent casting process. Hungerford[25] used solvent casting to make optically clear, oriented PI films with high electrical resistance, flexibility, and strength. Yabuta and Akahori[30] favored solvent casting to prevent air bubbles and uneven film thickness. Okahashi et al.[31] made isotropic PI films by solvent casting process. Asakura et al.[32] also used solvent casting to produce aromatic PI films with high thermal and mechanical properties for flexible printed circuits and electrical insulated material. Kohn[33] prepared ultrathin and pinhole-free PI films with fluorinated PI solution on water by solvent casting process.

The basic sketch of a standard solution casting line is displayed in Figure 1; a polymer solution ready for casting is emanating from a slit die (A) that is set vertically downward, the liquid film is deposited on a highly polished moving steel belt (B), this film on the belt will be dried in the oven (C) to remove solvents. Once the film is almost dried, it will be peeled off from the steel belt at point (D), and then the peeled film will go through a series of post-treatment such as tentering for post-curing if necessary. Because the fluid motion in this region can

Applied Polymer SCIENCE

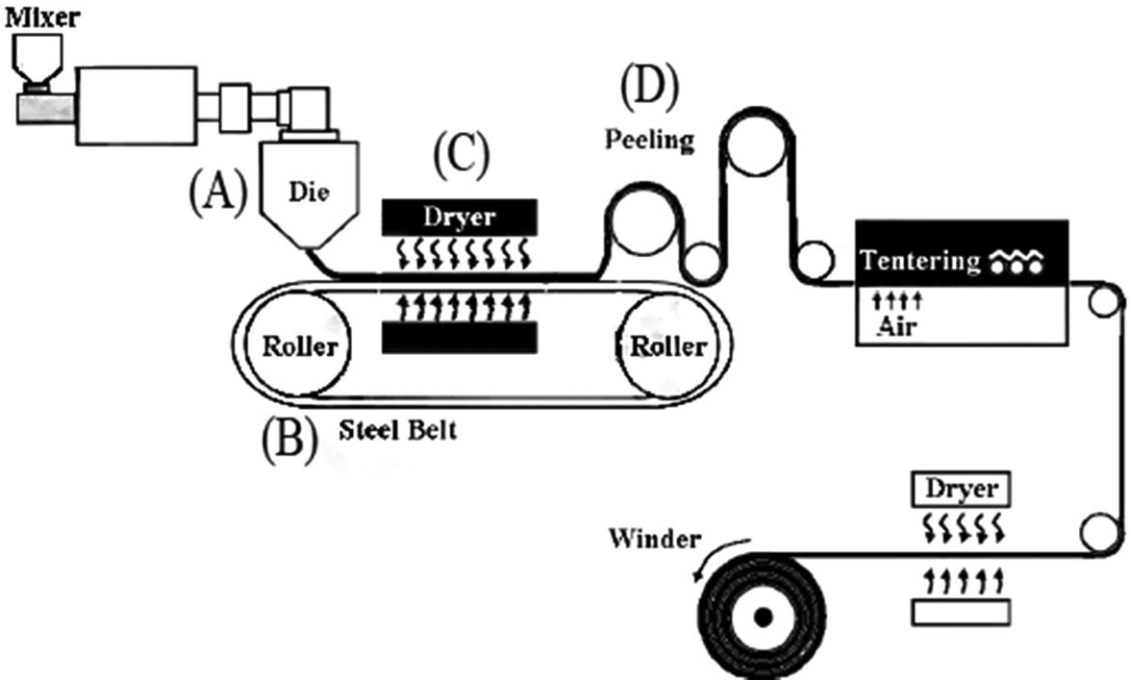

Figure 1. A basic sketch of a solution casting process.

decide if the stable operation is possible, this research is focused on the flow region between the slot die (A) exit and the moving belt (B). We used glycerol solutions rather than polymer solutions, and PET films rather than steel belts for convenience in the present analysis, the experimental results observed shall be qualitatively similar to actual industrial application. The results with polymeric liquids will appear in a subsequent article.

The fluid motion in the slot exit region is similar to those in the slot die and curtain coating operations. Analysis on these two types of coating operations can be found in several standard textbooks.[34,35] However, there are two major differences; the first is that the viscosity of the cast solution is usually much higher than those used in slot die and curtain coating operations. Another difference is the gap between the slot die and the moving belt is usually larger than the gap for slot die coating but smaller than the height of curtain coating operation. The edge guides to support the curtain usually are not required for solution casting. In the present analysis, we shall determine the operating window of solution casting for Newtonian fluids and also apply the flow visualization developed previously for slot die coating[36,37] to observe the fluid motion at the slot exit. Comparison of the performance of these two operations based on some previous works on slot die coating[36,37] and curtain coating[37,38] will also be presented.

EXPERIMENTAL

PET film of thickness 50 μm purchased from Nan Ya Plastic (BH-21) was used as the moving substrate. Aqueous glycerol solutions (Uni-onward, XR-LGLY-20L) were used as test fluids. The viscosities of the test fluids were measured with a rheometer (Brookfield, LVDP-III Ultra). Surface tension was detected by a surface tensiometer (Kyowa Interface Science, CBVP-A3). The measurement was based on the Wilhelmy Plate method. The instrument has a measuring range of 0–200 dyne/cm, with an accuracy of $\pm$0.1 dyne/cm. During the measurement, the temperature was controlled at 25°C using a circulated water bath. The wetting angles between the glycerol solutions and the PET substrate were determined by a AST Product machine (VCA-Optima XE). Physical properties of glycerol solutions are listed in Table I.

The photo of the experimental setup is shown in Figure 2. A roll of PET film is loaded on the unwinding roller O, this film will pass through several rollers for tension control purpose, and then it will reach a back roller Q. A slot die K setting

Table I. Physical Properties of Glycerol Fluids for the Solution Casting Experiment

	Viscosity (mPa s)	Density (g/cm^3)	Surface tension (mN/m)	Contact angle with die (°)	Contact angle with PET substrate (°)
A	110	1.231	63.2	92.2	70.7
B	132	1.231	62.4	91.0	69.1
C	180	1.233	62.4	92.1	70.3
D	250	1.233	62.4	90.3	66.3
E	295	1.236	62.4	90.3	65.7
F	340	1.241	62.5	89.0	68.1
G	450	1.245	62.5	91.3	68.5
H	600	1.248	62.4	94.1	68.1
I	820	1.256	63	90.4	69.7
J	1000	1259	63	91.7	67.9
K	1200	1.259	63.2	94.3	64.9

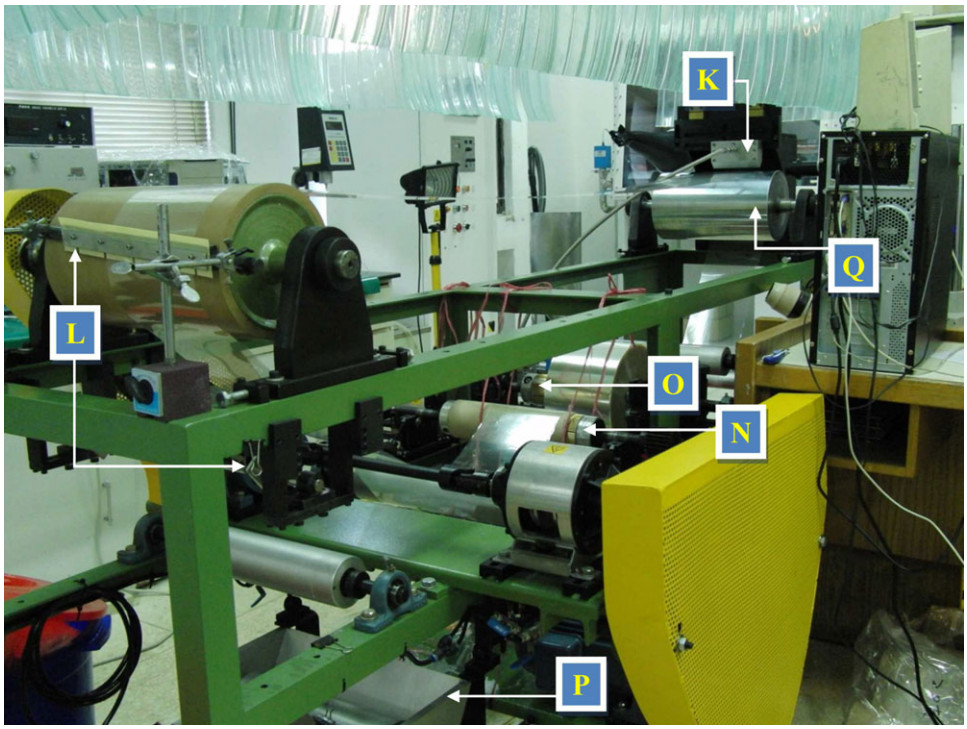

Figure 2. Photo of the experimental setup. O: unwinding roller; Q: back roller; K: slot die; L: blades; P: washing tank; N: winding roller. [Color figure can be viewed in the online issue, which is available at wileyonlinelibrary.com.]

vertically downward on the moving substrate will deliver the test fluid onto the substrate for observation. Several blades L will remove the fluid on the moving substrate, and then the film will go through a washing tank P before the final winding on the roller N. The slot die is critical for the flow experiment. A slot die was designed to deliver a uniform liquid sheet for the flow experiment. The photo and geometry of the slot die used in the present experiment are shown in Figure 3. The geometric parameters are listed in Table II. To observe the fluid motion in the neighborhood of the slot die, a CCD camera (Moritex, ML-Z07545) and a lighting source are placed close to the slot die as shown in Figure 4. Proper lighting is necessary to observe the two free surfaces of the flow domain clearly. The Photoshop software is necessary to improve the quality of the photos taken. During the flow experiment, the gap H_o between the slot die and the moving PET substrate was adjusted between 200 and 1000 μm. The substrate speed V changed from 1 m/min to the maximum speed 30 m/min.

RESULTS AND DISCUSSION

The objective of the present research is to find the operating windows of solution casting. The operating window is a stable domain in which defect-free casting operation is possible. Different types of defects would appear outside the operating window. Figure 5 displays the photos of different types of defects observed. A steady pool behind the slot die as shown in Figure 5(a) may appear at low speed. As the flow rate increases to a critical point, this heel will become unstable and starts to vibrate as shown in Figure 5(b), and the coated liquid surface

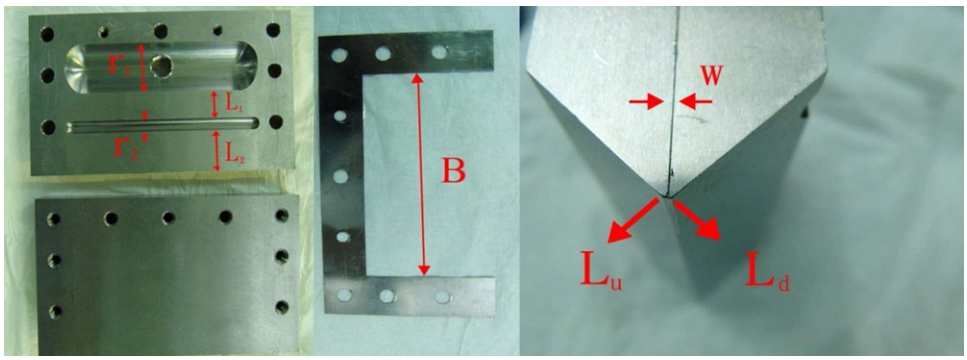

Figure 3. Photo and geometry of the slot die used in the experiment. [Color figure can be viewed in the online issue, which is available at wileyonlinelibrary.com.]

Applied Polymer SCIENCE

Table II. Geometric Parameters of the Slot Die

Variables	Dimension (mm)
Slot width, B	100
Slot gap, W	0.2
First slot length, L_1	8
Second slot length, L_2	20
Inner cavity radius, r_1	10
Inner cavity radius, r_2	3
Upstream die lip length, L_u	0.5
	1
Downstream die lip length, L_d	0.2

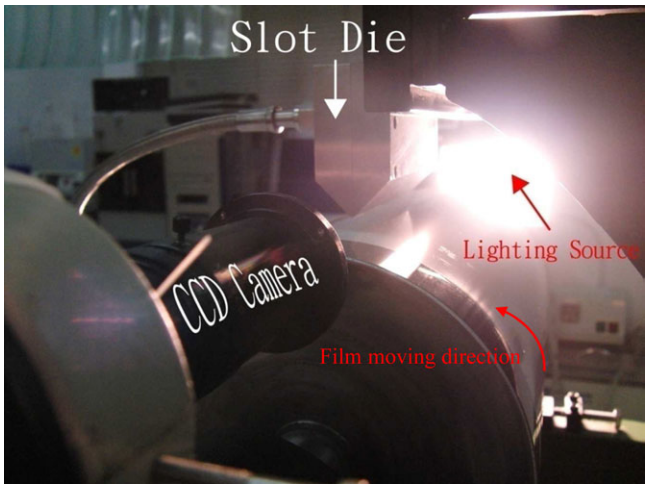

Figure 4. Setup for flow visualization. [Color figure can be viewed in the online issue, which is available at wileyonlinelibrary.com.]

also becomes irregular as shown in Figure 5(c). If the flow rate is low enough, the cast liquid film will either break into many rivulets as shown in Figure 5(d) for a small gap or vibrate the falling film and cause the edges of the liquid cast on the PET film to be irregular as shown in Figure 5(e) for a large gap. If the line speed is high enough, air bubbles are trapped into the liquid film as shown in Figure 5(f).

If the operating window is plotted as the flow rate/coating width q vs. the line speed V, different types of defects are marked outside the stable operating window as shown in Figure 6. The gap H_o is a critical parameter for stable costing: if $H_o <$ 600 μm, two general types of the operating windows can be observed as shown in Figure 6(a, b). The operating window in Figure 6(a) is for low-viscosity solutions ($\mu \leq 250$ mPa s). As the fluid viscosity increases, unstable pooling would appear at a lower flow rate and air entrainment may coexist with the unstable pooling as shown in Figure 6(b). If the gap is greater than 600 μm, unstable pooling disappears, but air entrainment may coexist with unstable pooling for high flow rates. We have found that the unstable pooling can be effectively postponed if

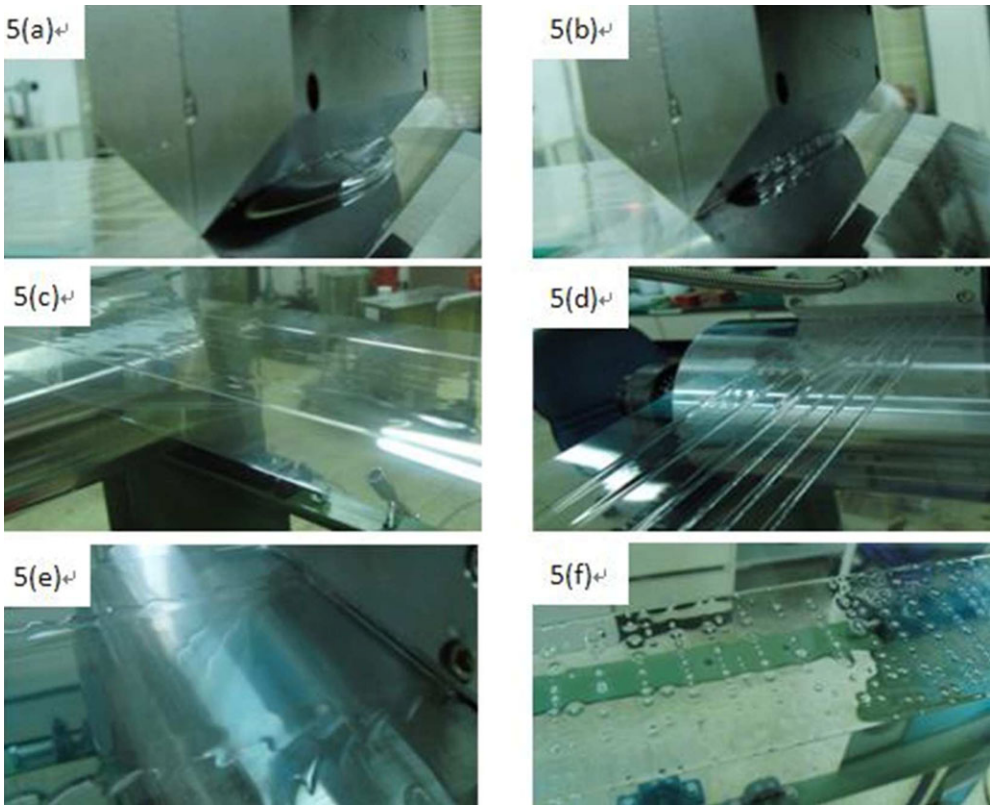

Figure 5. Photos of different types of defects outside the operating window: (a) pooling, (b) unstable pooling, (c) unstable pooling film, (d) rivulet, (e) vibrating, and (f) air entrainment. [Color figure can be viewed in the online issue, which is available at wileyonlinelibrary.com.]

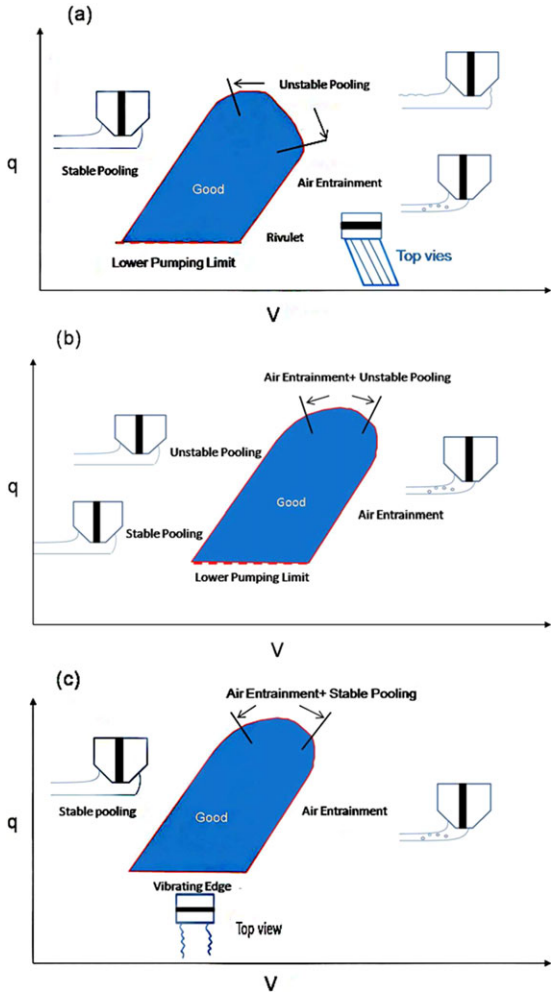

Figure 6. General presentation of operating window: (a) μ = 110–250 mPa s, H_o = 200–600 μm; (b) 295–1200 mPa s, H_o = 200–600 μm; and (c) μ = 110–1200 mPa s, H_o = 1000 μm. [Color figure can be viewed in the online issue, which is available at wileyonlinelibrary.com.]

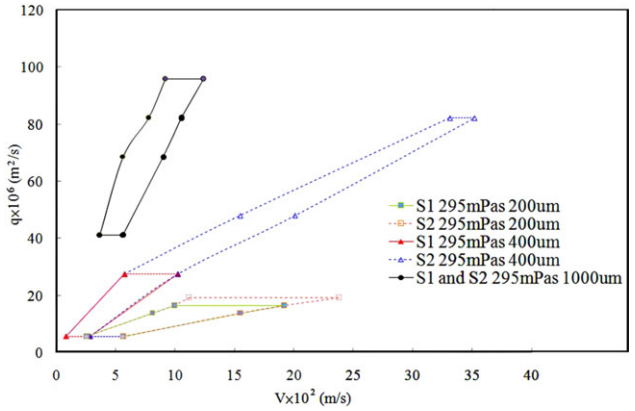

Figure 8. Comparison of the operating windows with two start-up approaches S_1 and S_2. [Color figure can be viewed in the online issue, which is available at wileyonlinelibrary.com.]

the upstream die lip length L_u is increased. Figure 7 displays the effect of increasing L_u from 500 to 1000 μm. Initially, the flow is stable as shown in Figure 7(a, b) for both cases with L_u equal to 500 and 1000 μm, respectively. As the line speed is decreased to $V = 13.0 \times 10^{-2}$ m/s, the flow with L_u equal to 500 μm becomes unstable and the upstream meniscus is left behind the upstream die lip as shown in Figure 7(c), unstable pooling appears. On the other hand, the flow as shown in Figure 7(d) remains stable at $V = 13.0 \times 10^{-2}$ m/s for the L_u = 1000 μm. Once an even lower line speed is reached, as $V = 8.5 \times 10^{-2}$ m/s, the flow becomes unstable as shown in Figure 7(e).

The effects of two different start-up approaches on the operating windows were examined first. The first approach S_1 is that the fluid emanating from the slot die starts to coat on the substrate at time $t = 0$ with the line speed of the substrate being zero. The line speed then starts from zero and increases to a specified value. On the other hand, the approach S_2 is that the solution starts to coat in the substrate only when the line speed of the substrate has already reached the specified value. S_1 and

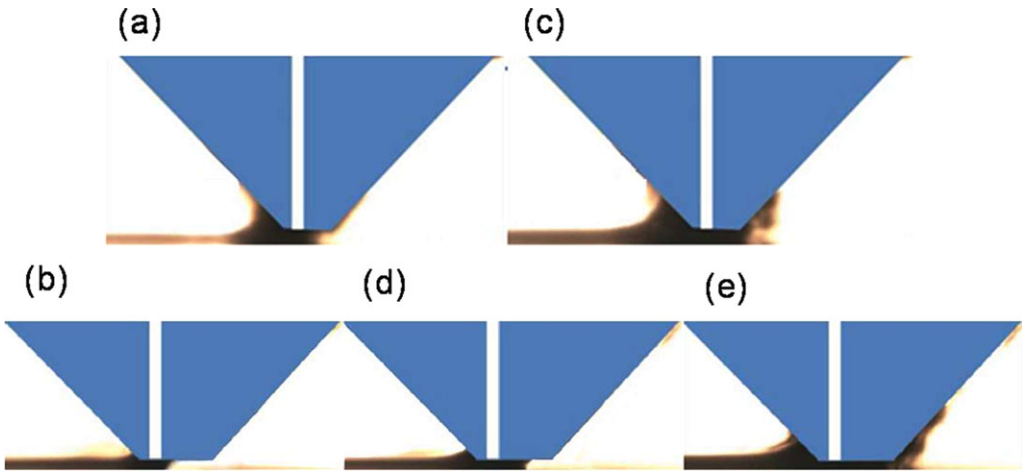

Figure 7. The effect of extending the upstream die lip L_u on unstable pooling: (a) L_u = 500 μm, $V = 21.0 \times 10^{-2}$ m/s, good film; (b) L_u = 1000 μm, $V = 21.0 \times 10^{-2}$ m/s, good film; (c) L_u = 500 μm, $V = 13.0 \times 10^{-2}$ m/s, unstable pooling; (d) L_u = 1000 μm, $V = 13.0 \times 10^{-2}$ m/s, good film; (e) L_u = 1000 μm, $V = 8.5 \times 10^{-2}$ m/s, unstable pooling. [Color figure can be viewed in the online issue, which is available at wileyonlinelibrary.com.]

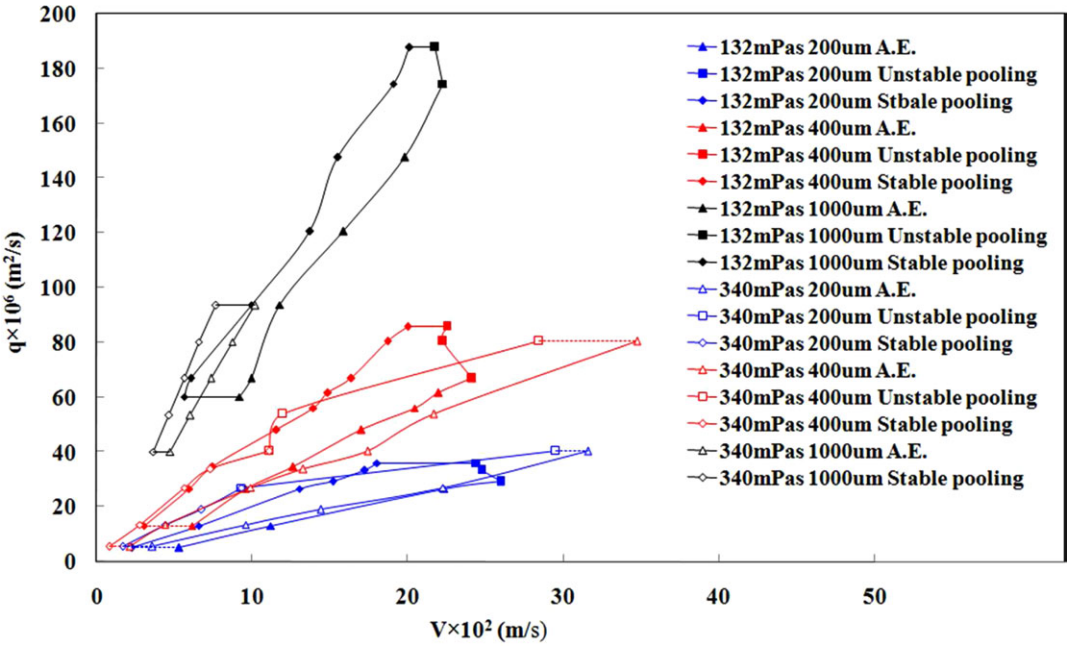

Figure 9. The effects of fluid viscosity and gap on the operating window. [Color figure can be viewed in the online issue, which is available at wileyonlinelibrary.com.]

S_2 are two limiting situations for industrial practice, usually the solution casting operation will start only when the line speed is slow (but not zero), then the flow rate will increase proportionally to the line speed until the specified wet thickness and line speed are both reached and then the steady operation will continue. It was found that if the viscosity of the solution is low, or the gap is large, the two approaches would generate the same operating window. On the other hand, if the viscosity is high, or the gap is small, the operating window generated by S_1 approach is much smaller than that generated by S_2. Figure 8 presents the operating window for the cast solution with viscosity $\mu = 295$ mPa s. If the gap is 1000 μm, the operating windows generated by the two approaches are identical. As the gap becomes smaller, it is not possible for S_1 to obtain stable coating at high flow rates and high speeds, because the solution accumulated in the neighborhood of the slot die exit cannot be taken to the downstream side by the moving web, owing to the high pressure required to pass the channel between the slot die

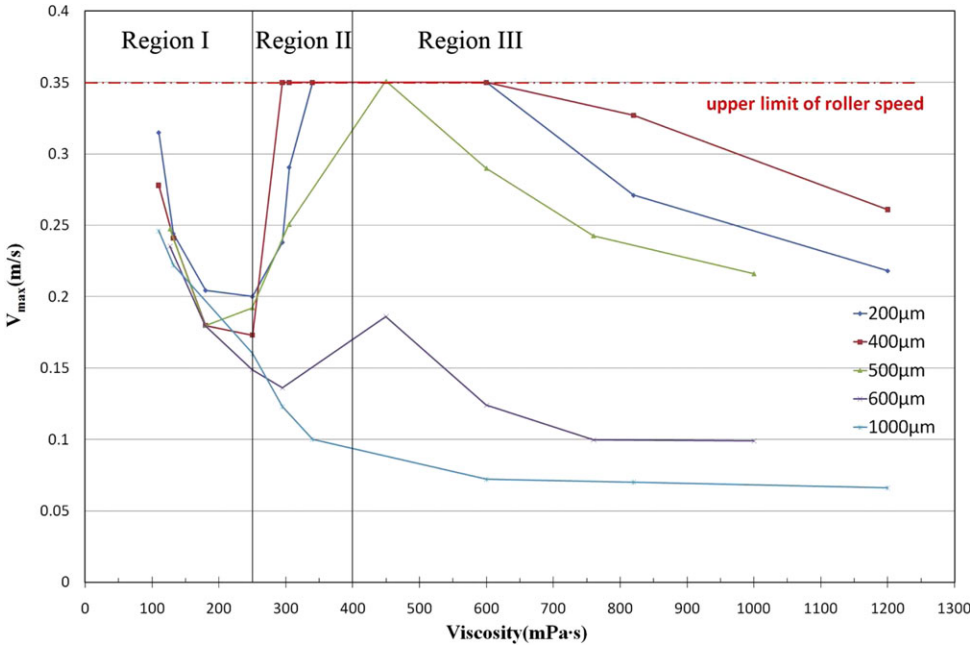

Figure 10. V_{max} for function of gap H_o and fluid viscosity μ. [Color figure can be viewed in the online issue, which is available at wileyonlinelibrary.com.]

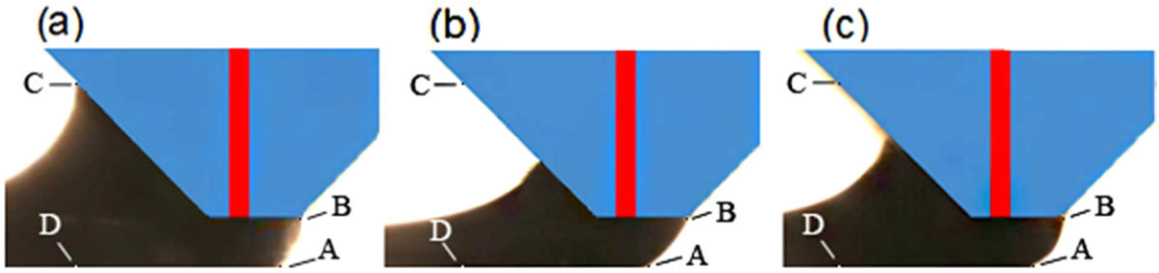

Figure 11. Photos of the flow domains in the slot exit for the three regions: (a) $\mu = 150$ mPa·s, (b) $\mu = 340$ mPa·s, and (c) $\mu = 900$ mPa·s. [Color figure can be viewed in the online issue, which is available at wileyonlinelibrary.com.]

and the moving substrate. For the gap, $H_o = 400$ μm, S_2 can generate a much larger operating window at high flow rate q and high speed. However, if the gap is reduced to 200 μm, the windows for these two approaches are much smaller and the difference becomes less significant.

Some typical operating windows obtained directly from the flow experiment are displayed in Figure 9, here solutions of two different viscosities were used, and the gap varied from 200 to 1000 μm. Usually a solution with a lower viscosity has a larger operating window. On the other hand, as the gap increases, the operating window would shift from a region of low flow rate and high line speed to a region of high flow rate and low line speed.

One of the key parameters for practical consideration is the maximum casting velocity V_{max} for stable operation. Figure 10 presents V_{max} as functions of the gap H_o and the fluid viscosity μ. It is interesting to note that if the gap H_o is greater than 600 μm, V_{max} goes down gradually as the fluid viscosity increases. The defect observed beyond V_{max} is air entrainment. The effect of viscosity and the defect observed are similar to those of slot die and curtain coatings.[36–38] However, if the gap H_o is smaller than 600 μm, it was found that V_{max} might go down and then go up as the fluid viscosity increases. Actually, there are three distinct regions. In Region I, V_{max} will go down as the fluid viscosity is increased until $\mu = 250$ mPa s, then V_{max} in Region II will go up as the fluid viscosity increases until $\mu = 450$ mPa s, V_{max} will go down again as the fluid viscosity is further increased in Region III. It is interesting to investigate why for a smaller gap H_o and in a certain range of viscosity, V_{max} will go up instead of going down as one may generally expect. The case of the gap $H_o = 500$ μm was selected for detailed analysis. The photos of the flow domains between the slot exit and the moving substrate for the three regions are displayed in Figure 11; it can be seen that the flow domain as shown in Figure 11(a) is similar to a coating bead in slot die coating operations in Region I and is relatively large when compared with other two cases. A previous study[36] found that coating flow is more stable if the coating bead is larger. On the other hand, the sizes of the flow domain in Regions II and III are compatible as shown in Figure 11(b, c). However, after careful measurement on the dynamic contact angles at point A in Regions II and III, it was found that the angles are close to 160° in Region III. Air entrainment would appear theoretically if the dynamic contact angle approaches 180°, a previous study found that the angle could be observed before air entrainment was 160°;[39] therefore, it implies that air entrainment is likely to appear in Region III.

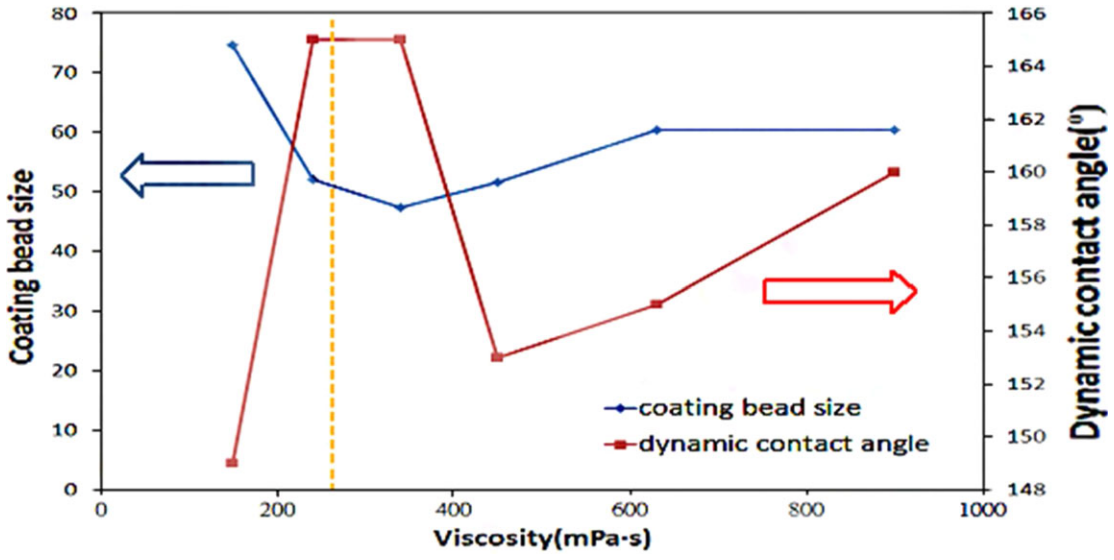

Figure 12. Estimated flow domain areas and the dynamic contact angles for $H_o = 500$ μm. [Color figure can be viewed in the online issue, which is available at wileyonlinelibrary.com.]

Applied Polymer SCIENCE

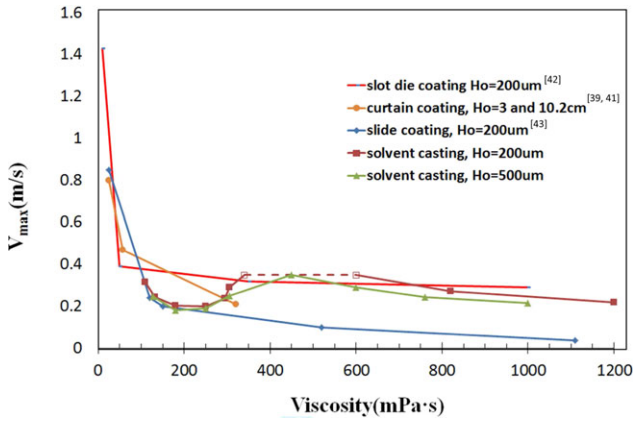

Figure 13. Comparison of V_{max} for different coating methods and solvent casting. [Color figure can be viewed in the online issue, which is available at wileyonlinelibrary.com.]

The areas of the flow domain can be measured from the four corners ABCD as shown in Figure 11. The areas of the flow domain together with the dynamic contact angles estimated from the photos for $H_o = 500$ μm as a function of fluid viscosity are given in Figure 12; it can be seen that the areas of the flow domain become smaller in Region I as the fluid viscosity increases and V_{max} drops, the areas of the domain increase gradually as the viscosity continues to increase in Region II and III, but the dynamic contact angle increases more rapidly and approaches 160°. Therefore, it is concluded that V_{max} is determined by two defects that are competing each other; if the flow domain becomes smaller, the flow is less stable, and unstable pooling would appear at a higher speed. On the other hand, once the dynamic contact angle approaches 160°, air entrainment would appear.

Data of V_{max} based on different coating methods and solvent casting are presented in Figure 13, the general trend is that as the fluid viscosity increases, V_{max} decreases, particularly in the low-viscosity regions. Curtain coating is not suitable for high-viscosity solutions.[40,41] On the other hand, the data of V_{max} for slot die coating[42] and solvent casting are relatively close. Slide coating[43] is usually not suitable for high-viscosity solutions; V_{max} becomes small for solutions with high viscosities. V_{max} would decrease as fluid viscosity increases for these three coating methods, which are different from solvent casting in the viscosity range between 250 and 600 mPa s.

There are five forces that may influence the casting flow, namely:

- viscous force F_v: $\mu V/H_0$
- surface tension force F_s: σ/H_0
- gravitational force F_g : $\rho g H_0$
- inertial force impinging on the moving web from the slot F_{Is}: $\rho V_s V_s$
- inertial force on the moving web F_{Iw}: ρVV

where V, V_s, ρ, and σ are the casting velocity, slot exiting liquid velocity, density, and surface tension, respectively. The effects of these five forces on V_{max} were analyzed for three different gaps. It was found that F_g and F_{Iw} are rather small for the cases we studied, therefore only the other three forces can be relevant.

Figure 14 presents the three forces calculated at V_{max} for solutions with different viscosities. The results in Figure 14(a) clearly indicate that only F_v and F_s are important for the cases with gap = 200 μm; therefore, a capillary number Ca $\equiv F_v/F_s$ is the only relevant dimensionless group that will influence V_{max}. The results for the gap $H_o = 500$ μm are displayed in Figure 14(b), if the fluid viscosity is lower than 295 mPa s, only two forces, i.e., F_{Is} and F_s are important; therefore, a Weber number We $\equiv F_{Is}/F_s$ can represent the influence of force on V_{max}. However, as μ is higher than 295 mPa s, all the three forces are relevant; consequently, in addition to the Weber number, capillary number Ca $\equiv F_v/F_s$ should be relevant, too. We have attempted to develop some universal correlations to relate

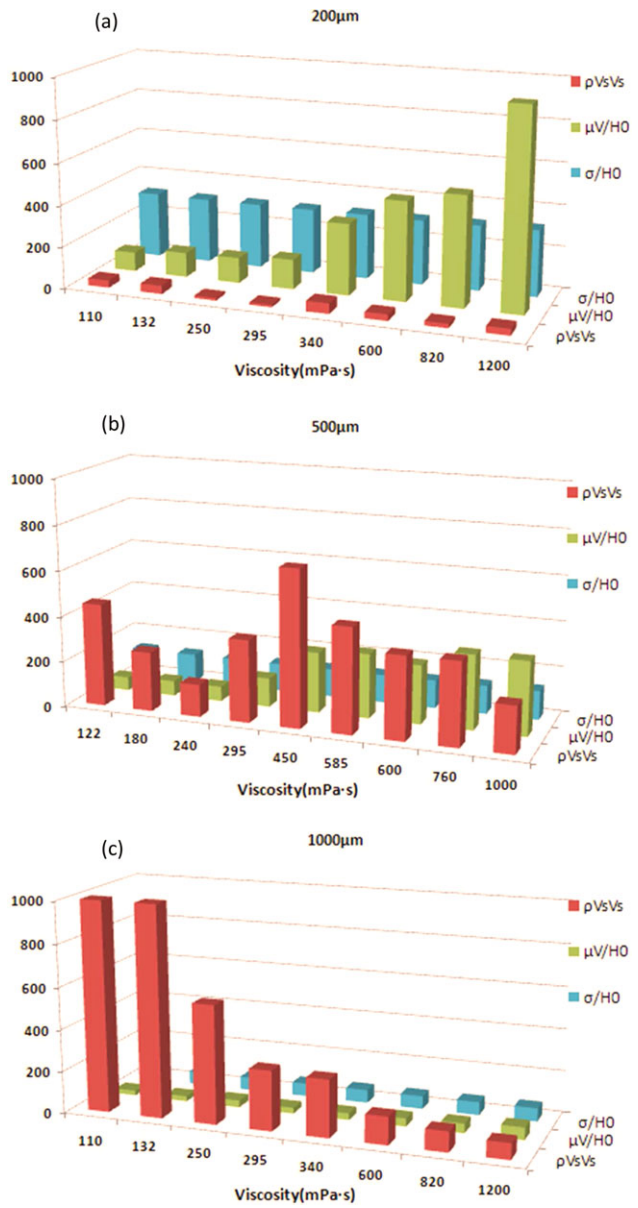

Figure 14. Comparison of three forces for three gaps: (a) $H_o = 200$ μm, (b) $H_o = 500$ μm, and (c) $H_o = 1000$ μm. [Color figure can be viewed in the online issue, which is available at wileyonlinelibrary.com.]

three dimensionless groups with V_{max}; the results are inclusive because it can be seen from Figure 14 that the ratios of forces change significantly, as the fluid viscosity varies.

CONCLUSIONS

We have carried out an experimental study to investigate the fluid mechanics of solution casting for Newtonian fluids. The emphasis is on evaluating the operating window as functions of different parameters. Different types of defects outside the operating windows were identified; unstable pooling and air entrainment were found to be the two significant defects that define the upper boundaries of the operating windows.

It was found that the two most critical parameters that influence the operating windows are the gap H_o between the slot die and the moving film substrate and the fluid viscosity μ. The operating window becomes smaller as the fluid viscosity increases. On the other hand, as the gap H_o increases, the maximum line speed V_{max} for stable casting would drop, but the flow rate for stable casting would increase.

We have also investigated the effects of the gap H_o and fluid viscosity μ on the V_{max} and found that if the gap H_o is greater than 600 μm, the only defect observed beyond V_{max} is air entrainment and V_{max} goes down as the fluid viscosity increases. On the other hand, if the gap is smaller than 600 μm, owing to the competition of two defects, i.e., unstable pooling and air entrainment, V_{max} may actually go up as the fluid viscosity increases from 250 to 450 mPa s. A dimensional analysis revealed that as the gap H_o varies, the importance of three forces on the flow could be identified.

ACKNOWLEDGMENTS

This research was supported by the National Science Council, ROC, under Grant No. NSC 98-2221-E-007-010-MY3.

REFERENCES

1. Underwood, W. F.; Craver, J. N.; Sacks, W. (to Union Carbide Corp.), US Pat. 3,337,665, August 22, **1967**.
2. Belcher, S. L. Practical Extrusion Blow Molding; Marcel Dekker: New York, **1999**; Chapter 3; p 63–74.
3. Han, C. D. Rheology in Polymer Processing; Academic Press: New York, **1976**; Chapters 9 and 10; p 238–283.
4. Middleman, S. Fundamentals of Polymer Processing; McGraw Hill: New York, **1977**; Chapters 6 and 10; p 123–163 and p 249–258.
5. Tadmor, Z.; Gogos, C. G. Principles of Polymer Processing, 2nd ed.; Wiley-Interscience: New York, **2006**; Chapters 6 and 14; p 235–298 and p 824–841.
6. Michaeli, W. Extrusion Dies; Hanser: New York, **1984**; Chapter 3; p 51–76.
7. Siemann, U. *Prog. Colloid. Polym. Sci.* **2005**, *130*, 1.
8. Shogo, F.; Nagayasu, K.; Masayoshi, S. (to Kaneka Corp.), Jpn. Pat. 2010077311, April 8, **2010**.
9. Kiyoshi, S.; Shinichi, M. (to Daicel Chemical Industries), Jpn. Pat. 2010163498, July 29, **2010**.
10. Takeshi, U.; Noboru, I.; Toshiyuki, N.; Eiji, M.; Keiichi, Y. (to Ube Industries), Jpn. Pat. 2010149494, July 8, **2010**.
11. Seiji, H.; Masayoshi, S.; Takashi, U.; Nagayasu, K. (to Kaneka Corp.), Jpn. Pat. 2011001439, January 6, **2011**.
12. Sakamaki, S. (to Fuji Photo Film Co.), WO Pat. 2006101186, September 28, **2006**.
13. Kojyu, I.; Satoshi, S. (to Fujifilm Corp.), US Pat. 0,099,954, May 1, **2008**.
14. Tsujimoto, T. (to Fuji Photo Film Co.), US Pat. 0,110,186, May 26, **2005**.
15. Miyaji, H. (to Fuji Photo Film Co.), Jpn. Pat. 2006027263, February 2, **2006**.
16. Akifumi, K.; Hidekazu, Y. (to Fuji Photo Film Co.), Jpn. Pat. 2007090866, April 12, **2007**.
17. Steven, J. H.; Lefferts, M. C. (to Celluloid Co.), US Pat. 573,928, December 29, **1896**.
18. Kinsella, E. (to Celanese Corp.), US Pat. 2,085,532, June 29, **1937**
19. Juergen, N.; Siemann, U. (to Lofo High Tech Film GmbH), WO Pat. 2004003062, January 8, **2004**.
20. Nakayama, H.; Fukakagawa, N.; Nishiura, Y.; Yasuda, T.; Ito, T.; Mihayashi K. *J. Photopolym. Sci. Tech.* **2006**, *19*, 169.
21. Higuchi, J.; Kato, M.; Suzuki, Y. (to Fuji Photo Film Co.), WO Pat. 2006095792, September 14, **2006**.
22. Satoshi, S. (to Fuji Photo Film Co.), WO Pat. 2006101186, September 8, **2006**.
23. Greener, J.; Lei, H.; Elman, J.; Chen, J. *J. Soc. Inf. Disp.* **2005**, *13*, 835.
24. Kim, H. T.; Kim, M. H.; Kim, B.; Koo, C. M.; Koo, K. K.; Hong, S. M. *Mol. Cryst. Liq. Cryst.* **2009**, *512*, 188.
25. Hungerford, G. P. (to Mobil Oil Corporation), US Pat. 4,405,550, September 20, **1993**.
26. Machell, J. S.; Greener, J.; Contestable, B. A. *Macromolecule* **1990**, *23*, 186.
27. Takeda, A. (to Konica Minolta Holdings), Jpn. Pat. 2009286929, December12, **2009**.
28. Law, P. W.; Longdon, A.; Willins, G. G. *Macromol. Symp.* **2004**, *208*, 293.
29. Hamamoto, T.; Inoue, H.; Miwa, Y.; Hirano, T.; Imatani, K.; Matsubara, K.; Kohno, T. (to Ube Industries, Ltd.), US Pat. 5,308,569, May 3, **1994**.
30. Yabuta, K.; Akahori, K. (to Kaneka Corporation), US Pat. 6,746,639, June 8, **2004**.
31. Okahashi, M.; Tsukuda, A.; Miwa, T.; Edman, J. R.; Paulson, C. M., II. US Pat. 5,324,475, **1994**.
32. Asakura, T.; Mizouchi, M.; Kobayashi, H. (to Toray Industries, Inc.), US Pat. 4,470,944, September 11, **1984**.
33. Kohn, R. S. (to Hoechst Celanese Corp.), US Pat. 4,929,405, May 29, **1990**.
34. Cohen, E. D.; Gutoff, E. B. Modern Coating and Drying Technology; Wiley-Interscience: New York, **1992**; Chapters 1 and 4; p 1–21 and p 117–167.

35. Kistler, S. F.; Schweizer, P. M. Liquid Film Coating: Scientific Principles and Their Technological Implications; Chapman & Hall: New York, **1997**; Chapter 11; p 399–536.

36. Chang, Y. R.; Chang, H. M.; Lin, C. F.; Liu, T. J.; Wu, P. Y. *J. Colloid Interface Sci.* **2007**, *308*, 222.

37. Chang, Y. R.; Lin, C. F.; Liu, T. *J. Polym. Eng. Sci.* **2009**, *49*, 1158.

38. Blake, T. D.; Clarke, A.; Ruschak, K. *J. AIChE J.* **1994**, *40*, 229.

39. Lin, C. F.; Wong, D. S. H.; Liu, T. J.; Wu, P. Y. *Adv. Polym. Tech.* **2010**, *29*, 31.

40. Blake, T. D.; Dobson, R. A.; Ruschak, K. J. *J. Colloid Interface Sci.* **2004**, *279*, 198.

41. Blake, T. D.; Bracke, M.; Shikhmurzaev, Y. D. *Phys. Fluids* **1999**, 11, **1995**.

42. Lee, K. Y.; Liu, L. D.; Liu, T. *J. Chem. Eng. Sci.* **1992**, *47*, 1703.

43. Gutoff, E. B.; Kendrick, C. E. *AIChE J.* **1987**, *33*, 141.